Molecular differences in APOBEC3 counteraction by primate herpesviruses reveal an evolutionary link between the genesis of APOBEC3B and novel viral ribonucleotide reductase function

Short title: APOBEC3 counteraction by herpesviruses

Sofia N. Moraes[1], Jordan T. Becker[1], Seyed A. Moghadasi[1], Nadine M. Shaban[1], Ashley A. Auerbach[1], Adam Z. Cheng[1], Reuben S. Harris[1,2,3,*]

[1] Department of Biochemistry, Molecular Biology, and Biophysics, Institute for Molecular Virology, Masonic Cancer Center, University of Minnesota; Minneapolis, MN 55455, USA.

[2] Department of Biochemistry and Structural Biology, University of Texas Health San Antonio, San Antonio, TX 78229, USA.

[3] Howard Hughes Medical Institute, University of Texas Health San Antonio, San Antonio, TX 78229, USA.

* Corresponding author. Email: rsh@umn.edu

Key words: APOBEC3A; APOBEC3B; evolutionary arms race; herpesvirus; host-pathogen interaction; innate immunity; restriction factor; ribonucleotide reductase; subcellular relocalization; viral evolution

Abstract

Viruses have evolved diverse mechanisms to antagonize host immunity. A recently discovered example is the direct inhibition and relocalization of cellular APOBEC3B (A3B) by the Epstein-Barr virus (EBV) ribonucleotide reductase (RNR) subunit BORF2. Recent reports also indicate interactions between the RNRs of other human herpesviruses and A3B, as well as interactions with the homologous APOBEC3A (A3A) enzyme. Here, we investigate the conservation of this APOBEC3 (A3) counteraction mechanism and reveal novel insights into its evolutionary origin. First, we found that herpesvirus RNRs bind to A3s via partially distinct surfaces. Second, we show that RNR-mediated relocalization and enzymatic inhibition of cellular A3s depend on binding to different regions of the A3 catalytic domain and that the inhibition is specific to A3B. Finally, we show that the ability of viral RNRs to counteract A3s is conserved in herpesviruses that infect humans and Old World monkeys, but absent in viruses infecting New World monkeys that naturally lack *A3B*. These results combine to indicate that the genesis of *A3B* at a critical branchpoint in primate evolution may have been a driving force in selecting herpesviruses with an expanded RNR functionality through counteraction of this antiviral enzyme.

Introduction

Cell-intrinsic innate immune proteins, or 'restriction factors', serve as the first line of defense against incoming viruses (reviewed by [1]). A prototypical example is the APOBEC3 (A3) family of single-stranded (ss)DNA cytosine deaminases, which provide broad and overlapping protection against viral infections (reviewed by [2, 3]). Classically, A3s exert their antiviral activity by catalyzing cytosine deamination in exposed ssDNA replication intermediates, often resulting in lethal mutagenesis of viral genomes. Humans encode seven A3 enzymes (A3A-D, A3F-H), which have been implicated in the restriction of retroviruses (HIV and HTLV) [4-8], endogenous retroviruses (HERV) [9, 10], hepadnaviruses (HBV) [11, 12], papillomaviruses (HPV) [13], polyomaviruses (BK) [14], and most recently the gamma-herpesvirus EBV [15]. It is difficult to predict which subset of A3 enzymes has the potential to restrict a given virus, but differences in the subcellular localization properties of these enzymes can provide useful insights into their antiviral targets. For instance, cytoplasmic A3s like A3G and A3F potently restrict HIV-1 by binding to viral genomic RNAs in the cytoplasm, packaging into budding virions at the cell membrane, and deaminating viral ssDNA intermediates during reverse transcription [16-18]. It thus follows that A3B—the only constitutively nuclear human A3 enzyme—may pose a threat to the genomic integrity of viruses that undergo replication in the nucleus, such as EBV and related herpesviruses.

Viruses that are susceptible to restriction by cellular A3s have evolved potent counteraction mechanisms to ensure successful replication (reviewed by [2, 3, 19]). The most well-studied A3 antagonist is the lentiviral accessory protein Vif, which nucleates the formation of an E3 ubiquitin ligase complex to promote the selective degradation of up to five different cytoplasmic A3s: A3C, A3D, A3F, A3G, and A3H (reviewed by [2, 20, 21]). Extensive mutagenesis analyses revealed

that HIV-1 Vif evolved to use distinct binding surfaces as a common solution to recognize different A3s, as underscored by separation-of-function mutants of Vif that selectively degrade only a subset of these enzymes (reviewed by [20, 22, 23]). These studies have been essential to our understanding of how viruses adapt to overcome innate host defenses and, collectively, highlight the importance of elucidating structure-function relationships between proteins at the host-pathogen interface.

HIV-1 and related retroviruses are thought to be the main viral targets of A3 enzymes due to obligate ssDNA replication intermediates, abundant evidence for A3-catalyzed hypermutation of viral genomes, and a potent A3 counteraction mechanism. Reports of DNA viruses exhibiting signatures of A3-mediated mutagenesis suggest that these viruses may also be susceptible to restriction by A3 enzymes [2, 24], although the identification of viral antagonists has been challenging. We recently discovered that the large double-stranded (ds)DNA herpesvirus Epstein-Barr Virus (EBV) uses a two-pronged approach to counteract the antiviral activity of A3B. The large subunit of the EBV ribonucleotide reductase (RNR), BORF2, directly inhibits A3B catalytic activity and relocalizes this enzyme from the nucleus to cytoplasmic aggregates—most likely to protect viral genomes from deamination during lytic replication ([15]; depicted in **Fig. 1A**). Consistent with this interpretation, BORF2-null EBV accumulates A3B signature C/G to T/A mutations upon lytic reactivation and exhibits significantly lower infectivity [15].

The deamination activity of all A3 family enzymes requires a zinc-coordinating motif, which forms the core of the catalytic site and is surrounded by three loop regions (L1, L3, and L7) that contribute to binding of ssDNA substrates [25-27]. These loops vary in size and amino acid composition and account for differences in A3 catalytic rates and local target sequence preferences (reviewed by [28, 29]; **Fig. 1B**). Each A3 enzyme is composed of single or double zinc-

coordinating (Z) domains that can be grouped into three classes (Z1, Z2, and Z3) based on sequence similarity [30]. In humans, A3A, A3C, and A3H are single Z domain proteins (Z1, Z2, and Z3, respectively), whereas A3B, A3G, A3D, and A3F harbor two Z domains (Z2-Z1 for A3B and A3G, Z2-Z2 for A3D and A3F) (depicted in **Fig. 1C**). The neutralization of A3B by EBV BORF2 is the first example of direct inhibition of A3 DNA deaminase activity by another protein, and our recently published cryo-EM structure of EBV BORF2 in complex with the C-terminal Z1 catalytic domain of A3B (A3Bctd) provides critical insights into the structural basis and molecular mechanism of this unanticipated host-pathogen interaction [31]. Specifically, our cryo-EM studies revealed that EBV BORF2 binds to the L1 and L7 regions of A3Bctd, resulting in a high-affinity interaction that effectively blocks the A3B active site from binding to ssDNA substrates and catalyzing deamination. Recently, we and others have shown that the RNR subunits from at least two additional human herpesviruses (KSHV ORF61 and HSV-1 ICP6) also bind and relocalize A3B—as well as the highly similar A3A enzyme—suggesting that this A3 counteraction mechanism may be conserved ([32-34]; **Fig. 1D**).

Here, we investigate the functional and mechanistic conservation of A3-neutralization by the RNR subunits of different herpesviruses using structurally and evolutionarily informed approaches. We found that the RNR subunits of EBV, KSHV, and HSV-1 interact with A3B and A3A by binding to distinct loop regions near the deaminase active site, which accounts for differences in binding selectivity and capacity to inhibit A3 enzymatic activity. We also uncovered potential coevolutionary interactions between A3 enzymes and primate herpesviruses by discovering a link between the generation of the *A3B* gene in primates and the evolution of A3-neutralization functionalities in herpesvirus RNRs. Our data provide evidence for a conserved A3

antagonist in primate gamma-herpesviruses and offer insights into how genetic conflicts with restriction factors may have affected the structure and function of herpesvirus proteins.

Results

Involvement of the A3B and A3A loop 7 regions in binding to herpesvirus RNRs

Recent biochemical and structural studies revealed that direct contacts between EBV BORF2 and the loop 7 (L7) region of A3Bctd are the major determinants of this host-pathogen interaction [15, 31]. The A3Bctd shares >90% amino acid sequence identity with A3A, including identical L7 regions (**Fig. 1B**), suggesting that a similar interaction with L7 residues could explain EBV BORF2 ability to bind and relocalize A3B and A3A, but not other A3 family members. Interestingly, previous work also revealed that the large subunit of the RNR from the closely related gamma-herpesvirus KSHV (ORF61) and the more distantly related alpha-herpesvirus HSV-1 (ICP6) similarly relocalize A3B and A3A, but not other A3s ([33]; **Fig. 1D**).

To address whether binding to L7 is a conserved requirement for viral RNR-A3 interaction, we generated a series of chimeric A3 proteins with reciprocal L7 swaps and tested their ability to bind to the different viral RNRs in co-immunoprecipitation (co-IP) experiments (**Fig. 2A**). 293T cells were transfected with FLAG-tagged viral RNRs and EGFP-tagged A3s, subjected to anti-FLAG affinity purification, and analyzed by immunoblotting. As expected from our prior studies, replacing L7 of A3Bctd or A3A with L7 of A3Gctd completely abolishes interaction with EBV BORF2 (**Fig. 2A**, upper panel, lanes 1-4) and, reciprocally, replacing L7 of A3Gctd with L7 of A3A/Bctd endows binding (**Fig. 2A**, upper panel, lanes 5-6). However, we were surprised to find that replacing L7 of A3Bctd or A3A with L7 of A3Gctd has little effect on pull-down by the RNR of the most closely related human gamma-herpesvirus, KSHV ORF61 (**Fig. 2A**, middle panel,

lanes 1-4). Accordingly, replacing L7 of A3Gctd with L7 of A3A/Bctd does not enable pull-down by KSHV ORF61 (**Fig. 2A**, middle panel, lanes 5-6). These results indicate that, despite a high degree of relatedness, the RNR subunits from EBV and KSHV appear to engage A3Bctd and A3A through at least partially distinct surfaces.

Slightly different phenotypes were also observed in co-IPs with the large subunit of the RNR of the more distantly related alpha-herpesvirus, HSV-1 ICP6 (**Fig. 2A**, lower panel). First, when compared to the gamma-herpesvirus RNRs, HSV-1 ICP6 interaction with A3Bctd (and potentially also A3A) appears to be substantially weaker, as evidenced by the low levels of protein pull-down (**Fig. 2A**, compare lanes 1 and 3 of the lower panel to the corresponding lanes of upper and middle panels). Second, like EBV BORF2, HSV-1 ICP6 interaction with A3Bctd and A3A appears to require L7, as replacing these regions with L7 of A3Gctd decreases pull-down (**Fig. 2A**, lower panel, lanes 1-4). Third, in contrast to results with EBV BORF2, grafting A3A/Bctd L7 into A3Gctd does not enable binding by HSV-1 ICP6 (**Fig. 2A**, lower panel, lanes 5-6). These results with L7 chimeric constructs combine to indicate that there is considerable variation in the interactions between these viral RNRs and A3Bctd, A3A, and A3Gctd.

A defining feature of the interaction between A3B/A and viral RNRs is relocalization from the nucleus to the cytoplasm ([15, 32, 33]; representative images in **Fig. 1D**). To evaluate the subcellular localization phenotypes of the L7 chimeras described above, we performed quantitative fluorescence microscopy experiments using HeLa cells co-transfected with EGFP-tagged A3s and FLAG-tagged viral RNRs (**Fig. 2B**, representative images). In agreement with our co-IP results, replacing L7 of A3Bctd or A3A with L7 of A3Gctd markedly decreases EBV BORF2-mediated relocalization (**Fig. 2B**, upper panel images; **Fig. 2C**, left) and, reciprocally, replacing L7 of A3Gctd with L7 of A3A/Bctd enables effective relocalization. Moreover, swapping L7 does not

substantially decrease KSHV ORF61-mediated relocalization of A3Bctd or A3A, nor does it increase A3Gctd relocalization (**Fig. 2B**, middle panel images; **Fig. 2C**, center). In further agreement with our co-IP results, the ability of HSV-1 ICP6 to relocalize A3Bctd and A3A is nearly abolished by replacing L7 with A3Gctd residues, whereas the reciprocal replacement of A3Gctd L7 shows no substantial effect (**Fig. 2B**, lower panel images; **Fig. 2C**, right).

Role of A3B and A3A loop 3 in binding to herpesvirus RNRs

Loop 3 (L3) is one of three loops that surround the A3 active site (**Fig. 1B**). In our recent cryo-EM studies of the EBV BORF2-A3Bctd complex, we were unable to model A3Bctd L3 residues due to the flexibility of this region [31]. Therefore, to functionally examine whether L3 participates in viral RNR-A3 interactions, we performed co-IP experiments using a panel of chimeric A3 proteins with reciprocal L3 swaps (**Fig. 3A**).

First, L3 appears dispensable for EBV BORF2 binding to A3Bctd and A3A, as indicated by similar pull-down levels for WT versus L3-swapped A3s (**Fig. 3A**, upper panel). Second, markedly distinct phenotypes are observed in co-IPs with KSHV ORF61, where replacing L3 of A3Bctd or A3A with L3 of A3Gctd completely abolishes the interaction (**Fig. 3A**, middle panel). However, replacing L3 of A3Gctd with L3 of A3A/Bctd is not sufficient to promote unambiguous immunoprecipitation with KSHV ORF61. Third, HSV-1 ICP6 binding to A3Bctd and A3A also appears to be at least partially dependent on interactions with L3, as replacing the L3 region of these enzymes with the corresponding region of A3Gctd markedly reduces pull-down by HSV-1 ICP6 (**Fig. 3A**, lower panel). Collectively, these results demonstrate that, while dispensable for EBV BORF2 binding, residues in A3Bctd and A3A L3 have critical roles in the interactions with both KSHV ORF61 and HSV-1 ICP6.

To evaluate the subcellular localization phenotypes of the L3 chimeras described above, we performed quantitative fluorescent microscopy experiments using HeLa cells (**Fig. 3B**, representative images). Similar to the L7 chimeras' results, microscopy observations were largely consistent with co-IP phenotypes. For EBV BORF2, L3 swaps have no substantial effect on relocalization (**Fig. 3B**, upper panel images; **Fig. 3C**, left). In contrast, replacing L3 of A3Bctd or A3A with the corresponding region of A3Gctd causes a marked decrease in relocalization by KSHV ORF61 and HSV-1 ICP6 (**Fig. 3B**, middle and lower panel images; **Fig. 3C**, center and right). Interestingly, despite the lack of visible co-IP (**Fig. 3A**, middle panel), KSHV ORF61 can relocalize the chimeric A3Gctd L3A/Bctd protein—albeit to a lesser extent compared to WT A3Bctd or A3A (**Fig. 3B**, middle panel images; **Fig. 3C**, center). This suggests that binding to an 'anchor' region (e.g., KSHV ORF61 interaction with L3) may be sufficient to initiate aggregate formation in living cells. Taken together, these results revealed unanticipated roles for the L3 region of A3Bctd and A3A in interacting with KSHV ORF61 and HSV-1 ICP6.

Role of A3B and A3A loop 1 in binding to herpesvirus RNRs

An unanticipated discovery made possible by our recent BORF2-A3Bctd cryo-EM structure is the existence of an extensive interaction between BORF2 and the loop 1 (L1) region of A3Bctd [31]. This interaction with L1 accounts for EBV BORF2 binding preferentially to A3B, as opposed to A3A, since the two proteins have identical L7 regions. We therefore accessed the role of L1 in A3Bctd versus A3A binding by the different herpesvirus RNRs. First, we confirmed our recent report by showing that grafting L1 of A3Bctd into A3A leads to a marked increase in EBV BORF2 co-IP (**Fig. 4A**, upper panel, lanes 1-2). A comparable increase in pull-down is also visible when L1 of A3A is replaced with L1 of A3Gctd, which can be explained by similarities

between the A3Bctd and A3Gctd L1 regions where both enzymes have a 3-residue motif that is absent in A3A (PLV and PWV, respectively, **Fig. 1B**). Reciprocally, replacing L1 of A3Bctd with L1 of A3A—but not with L1 of A3Gctd—dramatically diminishes the interaction with EBV BORF2 (**Fig. 4A**, upper panel, lanes 4-5).

In contrast, KSHV ORF61 and HSV-1 ICP6 do not appear to bind more strongly to A3Bctd compared to A3A (**Fig. 4A**, middle and lower panels, compare lanes 1 and 4). Moreover, L1 swaps between A3Bctd and A3A have no effect on KSHV ORF61 co-IPs (**Fig. 4A**, middle panel, lanes 1, 2, 4, and 5), indicating that this region may be dispensable for the interaction. Interestingly, replacing L1 of either A3Bctd or A3A with residues from A3Gctd prevents binding by KSHV ORF61 (**Fig. 4A**, middle panel, lanes 3 and 6). This can be explained by the presence of a bulky tryptophan residue in A3Gctd L1 potentially disrupting nearby interacting surfaces via steric hindrance (**Fig. 1B**). For HSV-1 ICP6, results resembled the pattern observed in co-IP experiments with L7 and L3 chimeras, with all L1 swaps causing marked decrease in pull-down strength (**Fig. 4A**, lower panel).

To evaluate the subcellular localization phenotypes of the L1 chimeras described here, quantitative fluorescence microscopy experiments were done using HeLa cells (**Fig. 4B**, representative images). For EBV BORF2, no overt changes in relocalization are observed when comparing WT versus L1 swapped A3Bctd and A3A (**Fig. 4B**, upper panels; **Fig. 4C**, left). Together with the data presented in **Fig. 2**, these results support the idea that L7 is the most critical determinant for EBV BORF2 binding to these cellular A3s, with L1 likely serving to help strengthen the interaction. For KSHV ORF61 and HSV-1 ICP6, swapping L1 of A3Bctd with L1 of A3Gctd decreases relocalization, whereas the remaining L1 swaps have little to no effect (**Fig. 4B**, middle and lower panels; **Fig. 4C**, center and right).

1

2 **Interaction with A3Bctd loop 1 is required for inhibiting DNA deaminase activity**

3 In addition to causing protein relocalization, the direct binding of EBV BORF2 potently inhibits
4 A3B catalytic activity *in vitro* [15, 31]. This supports a model in which BORF2 directly inhibits
5 and relocalizes A3B away from viral replication centers to protect EBV genomes from
6 deamination during lytic reactivation. Given results here showing that EBV BORF2, KSHV
7 ORF61, and HSV-1 ICP6 all bind to both A3Bctd and A3A, we next asked whether direct
8 enzymatic inhibition is a conserved feature of viral RNRs binding to these cellular enzymes.

9 Engineered HeLa T-REx cells stably expressing doxycycline-inducible A3B-EGFP or
10 A3A-EGFP were transfected with an empty vector control or FLAG-tagged EBV BORF2, KSHV
11 ORF61, or HSV-1 ICP6. After 24 hours of doxycycline induction, whole cell extracts were
12 incubated with a fluorescently labelled ssDNA oligonucleotide substrate containing a single
13 A3A/B deamination motif (5'-TC). A3B/A-mediated deamination of cytosine-to-uracil followed
14 by uracil excision by UDG and abasic site cleavage by sodium hydroxide (NaOH) yields a shorter
15 product that can be detected by SDS-PAGE and fluorescence scanning (**Fig. 5A**). As expected,
16 EBV BORF2 potently inhibits A3B deaminase activity, as evidenced by the near absence of a
17 product band (**Fig. 5A**, left panel, compare lanes 1-2). In contrast, KSHV ORF61 and HSV-1 ICP6
18 show little to no ability to inhibit A3B-catalyzed deamination when compared to a no-RNR control
19 (**Fig. 5A**, left panel, compare lane 1 to lanes 3 and 4). In addition, to our surprise, none of the three
20 viral RNRs substantially inhibits the deaminase activity of A3A (**Fig. 5A**, right panel).

21 This stark difference, at least for EBV BORF2, can be explained by our cryo-EM structure
22 showing extensive contacts between BORF2 and the L1 and L7 regions of A3Bctd, which results
23 in a high-affinity interaction that blocks the A3B active site from binding to ssDNA substrates and

catalyzing deamination ([31]; **Fig. 5B**, upper panel, and **Fig. 5C**). Specifically, A3B L1 residues 206-PLV-208 contribute to the formation of a hydrophobic pocket in which EBV BORF2 residue Y481 is inserted. In contrast, this 3-residue motif is absent in A3A L1 (**Fig. 1B**). We therefore hypothesized that inhibition of deaminase activity by EBV BORF2 requires not only binding to the catalytic domain through L7, but also a strong interaction with L1. To test this idea, we first generated mutants of EBV BORF2 Y481 and examined their ability to inhibit A3B-catalyzed deamination using engineered HeLa T-REx A3B-EGFP cells (**Fig. 5D**). Mutating EBV BORF2 Y481 to an alanine or a proline effectively prevents inhibition of A3B-catalyzed deamination, likely by weakening the interaction with the L1 region. Next, we compared the ability of EBV BORF2 to inhibit the deaminase activity of WT versus L1 swapped A3s in HeLa cells transfected with FLAG-tagged BORF2 and EGFP-tagged A3s. In agreement with results from **Fig. 5A**, WT A3B deaminase activity is potently inhibited by EBV BORF2 (**Fig. 5E**, left panel, lanes 1-2). In contrast, when L1 of A3B is replaced with L1 of A3A, EBV BORF2 loses its capacity to inhibit ssDNA deamination (**Fig. 5D**, left panel, lanes 3-4). In further agreement with **Fig. 5A**, WT A3A deaminase activity is not inhibited by EBV BORF2 (**Fig. 5D**, lanes 1-2). Unfortunately, the chimeric A3A L1B construct exhibits very low levels of DNA deaminase activity, and it was therefore not possible to determine the susceptibility of this protein to inhibition by EBV BORF2 (**Fig. 5D**, lanes 3-4). Nevertheless, these results combine to indicate that the EBV BORF2 interaction with A3B L1 is a requirement for inhibiting deamination and help to explain why A3A activity is not inhibited similarly.

Next, RoseTTAFold [35] was used to generate structural models of KSHV ORF61 and HSV-1 ICP6 for 3-dimensional comparisons (**Fig. S1**). Despite extensive amino acid differences (EBV BORF2 shares ~43% and ~34% amino acid identity with KSHV ORF61 and HSV-1 ICP6,

respectively), the structure of EBV BORF2 overlays well with the predicted RNR cores of KSHV ORF61 and HSV-1 ICP6 with root mean square deviation of 1.3 and 1.5 Å, respectively. Importantly, these structural superpositions indicate that a residue analogous to the interlocking Y481 of EBV BORF2 is lacking in KSHV ORF61 and HSV-1 ICP6 (**Fig. 5B**, middle and lower panels). Instead, both KSHV ORF61 and HSV-1 ICP6 have a proline (position 488 and 851, respectively) immediately downstream of conserved proline and threonine residues. This difference suggests that A3B L1 may be allowed to remain flexible and engage ssDNA substrates when bound by KSHV ORF61 and HSV-1 ICP6. Alternatively—and perhaps more likely—this lack of interaction with L1 may result in RNR-A3B complexes with lower affinity and consequently higher dissociation rates (compared to the EBV BORF2-A3B complex), thereby rendering KSHV ORF61 and HSV-1 ICP6 unable to prevent A3B-catalyzed deamination.

The genesis of *A3B* may have helped shaping herpesvirus RNR evolution

A3 genes are unique to placental mammals and the evolutionary history of the *A3* locus is marked by frequent expansions and contractions resulting from independent events of gene amplification, loss, and fusion [36-39]. For instance, in the primate lineage leading to humans the *A3* locus expanded from an ancestral 3 deaminase domain cluster to the present day 11 domain (7 gene) cluster. Interestingly, ancestral *A3* gene reconstructions have indicated that *A3B* is one of the youngest primate *A3* genes [37, 40]. Specifically, *A3B* was likely created by duplication of ancestral Z2 and Z1 deaminase domains in a common ancestor of catarrhine primates (*i.e.*, Old World monkeys and hominoids) and is consequently absent in New World monkeys (depicted in **Fig. 6A**). We therefore hypothesized that the functionality of the herpesvirus RNRs as innate immune evasion factors may have been selected by the emergence of *A3B*.

To test this idea, we cloned the RNR large subunit genes from representative gamma-herpesviruses that infect primates with A3B (EBV and KSHV, which infect humans; McHV-4 and McHV-5, which infect rhesus macaques) and related viruses that infect primates without A3B (CalHV-3 and SaHV-2, which infect marmosets and squirrel monkeys, respectively) (**Fig. 6B**). We then examined the RNRs from these different gamma-herpesviruses for their ability to bind human A3Bctd and A3A in co-IP experiments (**Fig. 6C**). In support of this hypothesis, only the RNRs from viruses that infect A3B-encoding primates (humans and rhesus macaques) pull-down A3Bctd and A3A (**Fig. 6C**, lanes 1-4, left and right panels). In contrast, RNRs from viruses that infect primates without A3B (marmosets and squirrel monkeys) are unable to pull-down either of these enzymes (**Fig. 6C**, lanes 5-6, left and right panels).

We next asked if these viral RNRs can relocalize human A3B and A3A. Engineered HeLa T-REx cells were transfected with FLAG-tagged viral RNRs and incubated with doxycycline to induce A3B-EGFP or A3A-EGFP expression (**Fig. 6D**). In agreement with co-IP results, only the RNRs from viruses that infect A3B-encoding primates relocalize these enzymes from the nucleus to the cytoplasm. Together, these results suggest that the ability to bind and relocalize cellular A3s is conserved within RNRs from gamma-herpesviruses that infect catarrhine primates. Moreover, despite having a similar predicted architecture when overlayed with the EBV BORF2 structure (model overlays in **Fig. S2**), the RNRs from viruses that infect New World monkeys that lack A3B are unable to bind or relocalize human A3B and A3A.

Finally, we tested if the different viral RNRs can inhibit the deaminase activity of human A3B, as well as A3A, using engineered HeLa T-REx cells (**Fig. 6E**). Consistent with our previous results, EBV BORF2 potently inhibits A3B (**Fig. 6E**, upper panel, lane 2). A similarly strong inhibition is seen for the RNR of rhesus macaque McHV-4 (**Fig. 6E**, upper panel, lane 3). The

RNRs from KSHV and rhesus macaque McHV-5 did not overtly affect the formation of a product band but appeared to slow down A3B-catalyzed deamination, as suggested by a stronger substrate band compared to the no-RNR control (**Fig. 6E**, upper panel, lanes 5 and 6). Most importantly, the RNRs from marmoset CalHV-3 and squirrel monkey SaHV-2 are both defective in inhibiting A3B activity (**Fig. 6E**, upper panel, lanes 4 and 7). Additionally, none of the viral RNRs tested here inhibits the activity of human A3A (**Fig. 6E**, lower panel). Collectively, our results suggest a link between the generation of *A3B* in the common ancestor of catarrhine primates and the evolution of A3-counteraction functionalities (*i.e.,* binding, relocalization, and enzymatic inhibition) in gamma-herpesvirus RNR subunits.

Discussion

Viruses use a plethora of mechanisms to avoid and antagonize host immune responses. We previously reported an unexpected role for herpesvirus RNRs in counteracting innate immunity by revealing that EBV repurposes its RNR subunit BORF2 to neutralize the antiviral activity of cellular A3B [15]. The importance of this A3B counteraction mechanism is evidenced by BORF2-null EBV exhibiting lower infectivity and an accumulation of A3B signature C/G-to-T/A mutations [15]. Subsequent studies revealed that the RNR subunits from related human herpesviruses also bind and relocalize A3B, as well as the highly similar A3A enzyme [32, 33]. Here, we leverage knowledge gained from our recent cryo-EM structure of EBV BORF2 in complex with the catalytic domain of A3B [31] to investigate the mechanistic conservation of A3 antagonism by herpesviruses. We find that EBV BORF2, KSHV ORF61, and HSV-1 ICP6 bind to cellular A3s via distinct surfaces. We also show that direct inhibition of DNA deaminase activity by EBV BORF2 requires specific interactions with the L1 of A3B in addition to the L7 region. We

further find that among primate gamma-herpesviruses, the existence of an RNR-mediated mechanism to counteract cellular A3s appears to be confined to viral species that infect A3B-expressing primate hosts. Together these results suggest that the genesis of *A3B* by duplication of ancestral Z2 and Z1 deaminase domains in the common ancestor of present-day hominoids and Old World monkeys may have selected for an ancestral herpesvirus with the capacity to counteract this new restriction factor through its large RNR subunit.

Our studies here highlight the overall conservation of A3 neutralization by herpesvirus large RNR subunits but also reveal new and unexpected molecular differences. In agreement with our recent cryo-EM studies [31], we show that A3A/B L7 is the most critical determinant of EBV BORF2 binding, whereas A3B L1 serves to help strengthen this interaction and confer selective binding (over A3A and A3G; **Fig. 2** and **Fig. 4**). Surprisingly, these same rules do not apply to other human herpesvirus RNRs. First, preferential binding to A3Bctd over A3A is not observed for KSHV ORF61 or HSV-1 ICP6 (**Fig. 4**). Second, although all three human herpesvirus RNRs interact with loop regions near the A3 active site, there is considerable variability in which loops are bound by the different viral proteins (**Figs. 2-4**). For instance, we found that L3—which is completely dispensable for EBV BORF2 binding—is the main determinant of binding by KSHV ORF61. Additionally, interactions with all three loop regions appear to contribute to HSV-1 binding. Together, our results suggest a model where interactions with L3 and/or L7—which are identical in A3B and A3A, but not in any other members of the A3 family—enable herpesvirus RNRs to bind and relocalize both enzymes, whereas additional interacting regions (e.g., EBV BORF2 and A3B L1) may help confer selectivity and additional neutralization activity (e.g., potent inhibition of A3B DNA deaminase activity).

Present-day herpesviruses can be divided into alpha-, beta-, and gamma- subfamilies, which are estimated to have diverged 170 to 220 million years ago [41-43]. These subfamilies share 43 core genes that were presumably inherited from a common ancestral virus, including the RNR large subunit gene [44, 45]. Similarities between herpesvirus RNR genes and their cellular counterparts suggest that the former were captured from the host [46, 47], but it has been unclear when additional functions may have been acquired by herpesvirus RNR homologues [48]. Our data suggest that the repurposing of gamma-herpesvirus RNR large subunits as innate immune evasion factors may be a relatively recent event selected by the generation of *A3B* in the common ancestor of catarrhine primates around 29 to 43 million years ago (**Fig. 6**). We show that, despite being predicted to have an overall organization and structure that is similar to EBV BORF2 (**Fig. S2**), the RNR large subunits from marmoset CalHV-3 and squirrel monkey SaHV-2 fail to bind, relocalize, or inhibit human A3B and A3A. In contrast, the RNRs large subunits from rhesus macaque McHV-4 and McHV-5 behave similarly to their human herpesvirus counterparts (EBV and KSHV, respectively) regarding their ability to counteract A3B and A3A. These results demonstrate that, within a same genus (*Lymphocryptovirus*: EBV, McHV-4, and CalHV-3; *Rhadinovirus*: KSHV, McHV-5, and SaHV-2), RNR-mediated counteraction of cellular A3s is confined to viruses that are adapted to infect and replicate in host species that express A3B. Moreover, the RNR subunits from all four human and rhesus macaque show some level of A3B inhibition—strong inhibition by EBV and McHV-4 RNRs, weak inhibition by KSHV and McHV-5 RNRs—but none was capable of inhibiting A3A, consistent with a model where the antiviral activity of A3B may have forced these viruses to evolve and maintain a potent counteraction mechanism. In comparison, the interaction with A3A may be a consequence of sequence homology to A3B and less likely a true physiologic function.

The A3B-selective nature of this host-pathogen interaction is further supported by previous binding studies showing that the EBV BORF2-A3Bctd interaction has a biolayer interferometry dissociation constant of ~1 nM, whereas the interaction with the > 90% identical A3A enzyme is over 10-fold weaker [31]. Our results here reveal that, in addition to providing selective binding to A3B, EBV BORF2 interaction with the L1 region of A3B is required for potently inhibiting DNA deaminase activity (**Fig. 5**). It is thus possible that the direct binding of EBV BORF2 to two loop regions near the A3B catalytic site—L1 and L7—helps stabilize the BORF2-A3B complex, resulting in low dissociation rates and consequently blocking the A3B active site from accessing ssDNA substrates and catalyzing deamination. In comparison, KSHV ORF61 binding to a single loop region of A3B (i.e., L3) presumably results in lower affinity and weakens its inhibitory effect on A3B-catalyzed DNA deamination. These inferences are consistent with a model in which binding to the A3 active site by viral RNRs is responsible for both protein relocalization and enzymatic inhibition, yet substantial deaminase activity inhibition is only observed above a certain affinity threshold. We therefore postulate that preferential binding to A3B might have been an evolutionary adaptation resulting from selective pressures disproportionally affecting gamma-herpesviruses within the *Lymphocryptovirus* genus, such as EBV and McHV-4. For instance, EBV latency is limited to B lymphocytes [49], which can express high levels of endogenous A3B [50, 51], implying that the neutralization of this enzyme is required to preserve viral genome integrity upon lytic reactivation. On the other hand, the broader tropism of KSHV suggests that lytic replication might not always occur in the presence of A3B [52-56], which potentially results in lower exposure to A3B-mediated deamination.

Evolutionary analyses of host-pathogen antagonistic relationships are powerful tools for understanding protein function. The link between *A3B* generation by duplication of ancestral Z2

and Z1 domains and the evolution of A3-neutralization functionalities in herpesvirus RNRs described here suggests that the double domain architecture of A3B may be a requirement for herpesvirus restriction. Notably, the catalytically inactive Z2 domain of A3B has been shown to account for this enzyme's distinct nuclear localization [57] and association with multiple nuclear RNA binding proteins, in addition to allosterically regulating the catalytic activity of the Z1 domain [58]. It is therefore plausible that cooperation between Z2 and Z1 accounts for A3B antiviral function, possibly by facilitating access to herpesvirus transcription complexes inside the nucleus (e.g., ssDNA exposed in viral R-loop structures [59]). Future studies dissecting the molecular mechanisms that allow A3B to recognize and target foreign nucleic acids such as herpesvirus genomes might reveal insights into the regulation of A3 DNA deaminase activity and how the loss of such regulatory mechanisms can at times result in cellular DNA mutations and cancer development (reviewed by [60, 61]). Additionally, a broader understanding of the evolutionary history of the interaction between different A3s and viral RNRs can help inform evolution-guided functional studies addressing the past and future of this potentially ongoing genetic conflict. Future work will likely benefit from interrogating the RNRs and A3 enzymes from a larger and more diverse panel of viral and host species, which is currently prevented by the low number of herpesvirus genomes deposited in public databases. Bat species in particular would be of great interest given they encode one of the largest A3 repertoires [62, 63] and are known hosts of dozens of different herpesviruses [64-74].

Materials and methods

DNA constructs

EBV BORF2, KSHV ORF61, HSV-1 UL39 (encodes ICP6), McHV-4 BORF2, McHV-5 ORF61, CalHV-3 ORF55, and SaHV-2 ORF61 were PCR amplified from gBlocks purchased from Integrated DNA Technologies and cloned into pcDNA4/TO (Invitrogen #V102020) with a C-terminal 3×FLAG-tag (DYKDDDDK). EBV BORF2$_{Y481A}$ and EBV BORF2$_{Y481P}$ constructs were generated by site-directed mutagenesis.

Full-length A3B, A3Bctd$_{193-382}$, full-length A3A, and A3Gctd$_{197-384}$ were cloned into pcDNA5/TO (Invitrogen #V103320) with a C-terminal EGFP-tag, as described previously [75]. The loop swap constructs A3B_L1A3A$_{25-30}$, A3Bctd$_{193-382}$_L1A3A$_{25-30}$, A3Bctd$_{193-382}$_L1A3G$_{209-217}$, A3Bctd$_{193-382}$_L3A3G$_{247-254}$, A3Bctd$_{193-382}$_L7A3G$_{317-322}$, A3A_L1A3B$_{205-213}$, A3A_L1A3G$_{209-217}$, A3A_ L3A3G$_{247-254}$, A3A_L7A3G$_{317-322}$, A3Gctd$_{197-384}$_L3A3A$_{60-67}$, and A3Gctd$_{197-384}$_L7A3A$_{132-137}$ were generated by site-directed mutagenesis.

Q5 High-Fidelity DNA Polymerase (NEB #M0491) was used for site-directed mutagenesis and Phusion High-Fidelity DNA Polymerase (ThermoFisher #F530L) was used for all other PCR reactions. All constructs were sequence confirmed using Sanger sequencing. Wild-type constructs match the following GenBank accessions: EBV BORF2 (V01555.2), KSHV ORF61 (U75698.1), HSV-1 UL39 (JN555585.1), McHV-4 BORF2 (AY037858.1), McHV-5 ORF61 (AF083501.3), CalHV-3 ORF55 (AF319782.2), SaHV-2 ORF61 (X64346.1), A3B (NM_004900), A3A (NM_145699), and A3G (NM_021822).

Human cell culture

Unless indicated, cell lines were derived from established laboratory collections. All cell cultures were supplemented with 10% fetal bovine serum (Gibco #26140-079), 1× penicillin-streptomycin (Gibco #15140-122), and periodically tested for mycoplasma contamination using

MycoAlert PLUS Mycoplasma Detection Kit (Lonza #LT07-710). 293T cells were cultured in high glucose DMEM (HyClone #SH30022.01) and HeLa cells were cultured in RPMI 1640 (Gibco #11875-093)

To generate HeLa T-REx A3A-EGFP and A3B-EGFP cell lines, HeLa cells were transduced with pLENTI6/TR (Invitrogen #V480-20), selected with 5 µg/ml blasticidin (GoldBio #B-800-25), and subcloned by serial dilution to obtain single cell clones. Clonal populations were stably transfected with pcDNA5/TO-A3A-EGFP or pcDNA5/TO-A3B-EGFP, selected with 200 µg/ml hygromycin (GoldBio #H-270-1), and subcloned by serial dilution. Representative clones were used for DNA deaminase activity assays (**Fig. 5A**, **Fig. 5D**, and **Fig. 6E**) and IF microscopy experiments (**Fig. 1D** and **Fig. 6D**).

Co-immunoprecipitation experiments

Approximately 250,000 293T cells were seeded in 6-well plates and transfected the next day with 100 ng pcDNA5/TO-A3-EGFP and 200 ng pcDNA4/TO-RNR-3×FLAG using TransIT-LT1 (Mirus #2304). Cells were harvested ~24 hours after transfection and resuspended in 500 µl of lysis buffer (50 mM Tris-HCl pH 7.4, 150 mM NaCl, 10% glycerol, 0.5% IGEPAL, 100 µg/ml RNaseA, 1 tablet of Sigma-Aldrich cOmplete Protease Inhibitor Cocktail). Resuspensions were vortexed, sonicated on ice-bath for 10 seconds at the lowest setting using a Branson sonifier, and centrifuged at 15,000 × g at 4 °C for 15 minutes. A 50 µl aliquot was removed from each sample for input detection and the remaining clarified whole cell lysate was incubated with 20 µl packed gel volume of anti-FLAG M2 magnetic beads (Sigma-Aldrich #M8823) at 4 °C overnight with gentle rotation. Samples were washed 3 times with 500 µL of lysis buffer and bound protein was eluted with 50 µl of elution buffer (100 µg/mL FLAG peptide (Sigma-Aldrich #F3290), 50 mM

Tris-HCl pH 7.4, 150 mM NaCl). Input and elution samples were analyzed by immunoblot using mouse anti-GFP (1:5,000, Clontech #632381) to detect A3-EGFP, rabbit anti-FLAG (1:5,000, Sigma-Aldrich #F7425) to detect RNR-3×FLAG, and rabbit anti-GAPDH (1:5,000, Proteintech #60004) to detect GAPDH (loading control). Secondary antibodies used were IRDye 800CW anti-rabbit (LI-COR #926-32211) and HRP-linked anti-mouse (Cell Signaling #7076), both at 1:10,000 dilution.

Immunofluorescence microscopy experiments

In **Fig. 1D** and **Fig. 6D**, approximately 5,000 engineered HeLa T-REx cells (described above) were seeded into 96-well imaging plates (Corning #3904) and transfected the next day with 30 ng pcDNA4/TO-RNR-3×FLAG. A3B-EGFP or A3A-EGFP expression was induced 6 hours after transfection with 50 ng/mL doxycycline. Approximately 24 hours after induction, cells were fixed in 4% formaldehyde (ThermoFisher #28906), permeabilized in 0.2% Triton X-100 (Sigma-Aldrich #T8787) for 10 minutes and incubated in blocking buffer (2.8 mM KH2PO4, 7.2mM K2HPO4, 5% goat serum (Gibco #16210064), 5% glycerol, 1% cold water fish gelatin (Sigma-Aldrich #G7041), 0.04% sodium azide, pH 7.2) for 1 hour. Cells were then incubated with primary antibody mouse anti-FLAG (1:1,000, Sigma #F1804) overnight at 4 °C with gentle rocking to detect FLAG-tagged viral RNRs. The next day, cells were incubated with secondary antibody anti-mouse Alexa Fluor 594 (1:1,000, Invitrogen #A-11005) for 2 hours at room temperature protected from light and nuclei were counterstained with Hoechst 33342 (ThermoFisher #62249) for 10 minutes. Representative images were acquired using a Cytation 5 Cell Imaging Multi-Mode Reader (BioTek) at 20× magnification.

In **Figs. 2-4**, approximately 5,000 HeLa cells were seeded into 96-well imaging plates (Corning #3904) and transfected the next day with 15 ng pcDNA5/TO-A3-EGFP and 30 ng pcDNA4/TO-RNR-3×FLAG. Cells were fixed approximately 24 hours after transfection. Permeabilization, antibody staining, and nuclei counterstaining with Hoechst 33342 were performed as described above. Plates were imaged using a Cytation 5 Cell Imaging Multi-Mode Reader (BioTek) at 20× magnification using the automated imaging function to capture 50 non-overlapping images per well. Background subtraction was performed using Fiji [76] and images were analyzed using CellProfiler v4.2 [77]. A pipeline was generated to identify individual nuclei, trace cell boundaries, segment the cytoplasmic and nuclear compartments, and take measurements of intensity, texture, and correlation with other stains for each type of staining in each subcellular compartment. At least 100 cells were measured for each well. Measurements were exported to an SQLite database and CellProfiler Analyst v3.0 [78] was used for scoring phenotypes by machine learning in order to quantify the number of cells showing relocalized versus non-relocalized A3 within the population of RNR-expressing cells in each well. The percentage of cells with relocalized A3 was calculated for n = 3 independent experimental replicates (i.e., data generated from the analysis of cells seeded, transfected, and imaged on three different days).

DNA deaminase activity assays

In **Fig. 5A**, **Fig. 5D**, and **Fig. 6E**, approximately 250,000 HeLa T-REx cells stably expressing doxycycline-inducible A3B-EGFP or A3A-EGFP (described above) were seeded into 6-well plates and transfected the next day with 200 ng pcDNA4/TO-RNR-3×FLAG using TransIT-LT1 (Mirus #2304). A3B-EGFP or A3A-EGFP expression was induced 6 hours after transfection with 50 ng/mL doxycycline. Approximately 24 hours after induction, cells were harvested,

resuspended in 100 µL of reaction buffer (25 mM HEPES, 15 mM EDTA, 10% glycerol, 1 tablet of Sigma-Aldrich cOmplete Protease Inhibitor Cocktail), and subjected to freeze-thaw. Whole cell lysates were then centrifuged at 15,000 × g for 15 minutes and the clarified supernatant was transferred to a new tube. Soluble lysates were incubated with 100 µg/mL RNAse A at room temperature for 1 hour. A 5 µl aliquot was removed from each sample for immunoblots using mouse anti-GFP (1:5,000, Clontech #632381) to detect A3-EGFP, rabbit anti-FLAG (1:5,000, Sigma-Aldrich #F7425) to detect RNR-3×FLAG, and rabbit anti-GAPDH (1:5,000, Proteintech #60004) to detect GAPDH (loading control). Secondary antibodies used were IRDye 800CW anti-rabbit (LI-COR #926-32211) and HRP-linked anti-mouse (Cell Signaling #7076), both at 1:10,000 dilution. 5 µl of soluble lysate were incubated at 37 °C for 1 hour with 0.7 µM of a fluorescent oligo substrate (5′-ATT ATT ATT AT<u>T</u> <u>CA</u>A ATG GAT TTA TTT ATT TAT TTA TTT ATT T-fluorescein-3′) and 2.5 U of UDG (NEB #M0280) in a total reaction volume of 10 µl (diluted in reaction buffer). NaOH was then added to the reaction mix to a final concentration of 100 mM and samples were incubated at 98 °C for 10 minutes. The reaction was then mixed with 11 µl 2× formamide buffer (80% formamide, 1×TBE, bromophenol blue, and xylene cyanol) and reaction products were separated on a 15% TBE-urea PAGE gel. Separated DNA fragments were visualized on a Typhoon FLA 7000 scanner (GE Healthcare) on fluorescence mode.

In **Fig. 5E**, approximately 250,000 293T cells were seeded in 6-well plates and transfected the next day with 100 ng pcDNA5/TO-A3-EGFP and 200 ng pcDNA4/TO-EBV-BORF2-3×FLAG. Cells were harvested approximately 24 hours after transfection and the DNA deaminase activity assay proceeded as described above.

Herpesvirus phylogenetic tree generation

Amino acid sequences for the RNR large subunits from the following herpesviruses were obtained from the NCBI Protein RefSeq database: HSV-1 (YP_009137114.1), HSV-2 (YP_009137191.1), VZV (NP_040142.1), EBV (YP_401655.1), HCMV (YP_081503.1), HHV-6A (NP_042921.1), HHV-6B (NP_050209.1), HHV-7 (YP_073768.1), KSHV (YP_001129418.1), McHV-4 (YP_067953.1), McHV-5 (NP_570809.1), CalHV-3 (NP_733909.1), and SaHV-2 (NP_040263.1). Sequences were aligned using MUSCLE [79] and a phylogenetic tree was reconstructed by the neighbor-joining (NJ) method using MEGA X [80].

Acknowledgements

We thank members of the Harris lab for thoughtful comments during the development of this project. These studies were supported in part by grants to RSH from the National Institute for Allergy and Infectious Diseases (NIAID) R37-AI064046 and the National Cancer Institute (NCI) P01-CA234228. Salary support for SNM was provided by NIAID F31-AI161910 and subsequently by a grant to the University of Minnesota (SNM and RSH) from the Howard Hughes Medical Institute through the James H. Gilliam Fellowships for Advanced Study program. Salary support for JTB was provided by NIAID F32-AI147813. Salary support for NMS was provided by NIAID R56-AI150402. Salary support for AAA was provided by NIH T32-AI83196. RSH is the Ewing Halsell President's Council Distinguished Chair and an Investigator of the Howard Hughes Medical Institute. The authors have no competing interests to declare.

References

1. Duggal NK, Emerman M. Evolutionary conflicts between viruses and restriction factors shape immunity. Nature Reviews Immunology. 2012;12(10):687-95. Epub 2012/09/14. doi: 10.1038/nri3295. PubMed PMID: 22976433; PubMed Central PMCID: PMCPMC3690816.
2. Harris RS, Dudley JP. APOBECs and virus restriction. Virology. 2015;479-480:131-45. Epub 2015/03/26. doi: 10.1016/j.virol.2015.03.012. PubMed PMID: 25818029; PubMed Central PMCID: PMCPMC4424171.
3. Simon V, Bloch N, Landau NR. Intrinsic host restrictions to HIV-1 and mechanisms of viral escape. Nature Immunology. 2015;16(6):546-53.
4. Sheehy AM, Gaddis NC, Choi JD, Malim MH. Isolation of a human gene that inhibits HIV-1 infection and is suppressed by the viral Vif protein. Nature. 2002;418(6898):646-50. Epub 2002/07/14. doi: 10.1038/nature00939. PubMed PMID: 12167863.
5. Harris RS, Bishop KN, Sheehy AM, Craig HM, Petersen-Mahrt SK, Watt IN, Neuberger MS, Malim MH. DNA deamination mediates innate immunity to retroviral infection. Cell. 2003;113(6):803-9. doi: 10.1016/s0092-8674(03)00423-9. PubMed PMID: 12809610.
6. Wiegand HL, Doehle BP, Bogerd HP, Cullen BR. A second human antiretroviral factor, APOBEC3F, is suppressed by the HIV-1 and HIV-2 Vif proteins. The EMBO Journal. 2004;23(12):2451-8. doi: 10.1038/sj.emboj.7600246. PubMed Central PMCID: PMCPMC423288.
7. Sasada A, Takaori-Kondo A, Shirakawa K, Kobayashi M, Abudu A, Hishizawa M, Imada K, Tanaka Y, Uchiyama T. APOBEC3G targets human T-cell leukemia virus type 1. Retrovirology. 2005;2(1):32. doi: 10.1186/1742-4690-2-32.

8. Dang Y, Wang X, Esselman WJ, Zheng Y-H. Identification of APOBEC3DE as another antiretroviral factor from the human APOBEC family. Journal of Virology. 2006;80(21):10522-33. doi: 10.1128/JVI.01123-06.

9. Esnault C, Heidmann O, Delebecque F, Dewannieux M, Ribet D, Hance AJ, Heidmann T, Schwartz O. APOBEC3G cytidine deaminase inhibits retrotransposition of endogenous retroviruses. Nature. 2005;433(7024):430-3. doi: 10.1038/nature03238.

10. Lee YN, Malim MH, Bieniasz PD. Hypermutation of an ancient human retrovirus by APOBEC3G. Journal of Virology. 2008;82(17):8762-70.

11. Turelli P, Mangeat B, Jost S, Vianin S, Trono D. Inhibition of hepatitis B virus replication by APOBEC3G. Science. 2004;303(5665):1829. doi: 10.1126/science.1092066. PubMed PMID: 15031497.

12. Suspène R, Guétard D, Henry M, Sommer P, Wain-Hobson S, Vartanian J-P. Extensive editing of both hepatitis B virus DNA strands by APOBEC3 cytidine deaminases in vitro and in vivo. Proceedings of the National Academy of Sciences. 2005;102(23):8321-6. doi: 10.1073/pnas.0408223102.

13. Vartanian J-P, Guétard D, Henry M, Wain-Hobson S. Evidence for editing of human papillomavirus DNA by APOBEC3 in benign and precancerous lesions. Science. 2008;320(5873):230-3.

14. Peretti A, Geoghegan EM, Pastrana DV, Smola S, Feld P, Sauter M, Lohse S, Ramesh M, Lim ES, Wang D. Characterization of BK polyomaviruses from kidney transplant recipients suggests a role for APOBEC3 in driving in-host virus evolution. Cell Host & Microbe. 2018;23(5):628-35. e7.

15. Cheng AZ, Yockteng-Melgar J, Jarvis MC, Malik-Soni N, Borozan I, Carpenter MA, Mccann JL, Ebrahimi D, Shaban NM, Marcon E, Greenblatt J, Brown WL, Frappier L, Harris RS. Epstein–Barr virus BORF2 inhibits cellular APOBEC3B to preserve viral genome integrity. Nature Microbiology. 2019;4(1):78-88. doi: 10.1038/s41564-018-0284-6.

16. Harris RS, Liddament MT. Retroviral restriction by APOBEC proteins. Nature Reviews Immunology. 2004;4(11):868-77. doi: 10.1038/nri1489.

17. Mangeat B, Turelli P, Caron G, Friedli M, Perrin L, Trono D. Broad antiretroviral defence by human APOBEC3G through lethal editing of nascent reverse transcripts. Nature. 2003;424(6944):99-103. doi: 0.1038/nature01709.

18. Navarro F, Bollman B, Chen H, König R, Yu Q, Chiles K, Landau NR. Complementary function of the two catalytic domains of APOBEC3G. Virology. 2005;333(2):374-86. doi: 10.1016/j.virol.2005.01.011.

19. Malim MH, Bieniasz PD. HIV restriction factors and mechanisms of evasion. Cold Spring Harbor Perspectives in Medicine. 2012;2(5):a006940.

20. Hu Y, Knecht KM, Shen Q, Xiong Y. Multifaceted HIV-1 Vif interactions with human E3 ubiquitin ligase and APOBEC3s. The FEBS journal. 2021;288(11):3407-17.

21. Uriu K, Kosugi Y, Ito J, Sato K. The battle between retroviruses and APOBEC3 genes: its past and present. Viruses. 2021;13(1):124.

22. Kitamura S, Ode H, Iwatani Y. Structural features of antiviral APOBEC3 proteins are linked to their functional activities. Frontiers in Microbiology. 2011;2:258.

23. Aydin H, Taylor MW, Lee JE. Structure-guided analysis of the human APOBEC3-HIV restrictome. Structure. 2014;22(5):668-84.

24. Shapiro M, Krug LT, MacCarthy T. Mutational pressure by host APOBEC3s more strongly affects genes expressed early in the lytic phase of herpes simplex virus-1 (HSV-1) and human polyomavirus (HPyV) infection. PLoS Pathogens. 2021;17(4):e1009560.

25. Shi K, Carpenter MA, Banerjee S, Shaban NM, Kurahashi K, Salamango DJ, McCann JL, Starrett GJ, Duffy JV, Demir Ö, Amaro RE, Harki DA, Harris RS, Aihara H. Structural basis for targeted DNA cytosine deamination and mutagenesis by APOBEC3A and APOBEC3B. Nature Structural & Molecular Biology. 2017;24(2):131-9. Epub 2016/12/19. doi: 10.1038/nsmb.3344. PubMed PMID: 27991903; PubMed Central PMCID: PMCPMC5296220.

26. Kouno T, Silvas TV, Hilbert BJ, Shandilya S, Bohn MF, Kelch BA, Royer WE, Somasundaran M, Kurt Yilmaz N, Matsuo H. Crystal structure of APOBEC3A bound to single-stranded DNA reveals structural basis for cytidine deamination and specificity. Nature Communications. 2017;8(1):1-8.

27. Maiti A, Myint W, Kanai T, Delviks-Frankenberry K, Sierra Rodriguez C, Pathak VK, Schiffer CA, Matsuo H. Crystal structure of the catalytic domain of HIV-1 restriction factor APOBEC3G in complex with ssDNA. Nature Communications. 2018;9(1):1-11.

28. Silvas TV, Schiffer CA. APOBEC3s: DNA-editing human cytidine deaminases. Protein Science. 2019;28(9):1552-66.

29. Maiti A, Hou S, Schiffer CA, Matsuo H. Interactions of APOBEC3s with DNA and RNA. Current Opinion in Structural Biology. 2021;67:195-204.

30. Larue RS, Andrésdóttir V, Blanchard Y, Conticello SG, Derse D, Emerman M, Greene WC, Jónsson SNR, Landau NR, Löchelt M, Malik HS, Malim MH, MüNk C, O'Brien SJ, Pathak VK, Strebel K, Wain-Hobson S, Yu X-F, Yuhki N, Harris RS. Guidelines for Naming

1 Nonprimate APOBEC3 Genes and Proteins. Journal of Virology. 2009;83(2):494-7. doi:
2 10.1128/jvi.01976-08.
3 31. Shaban NM, Yan R, Shi K, Moraes SN, Cheng AZ, Carpenter MA, Mclellan JS, Yu Z,
4 Harris RS. CryoEM structure of the EBV ribonucleotide reductase BORF2 and mechanism of
5 APOBEC3B inhibition. bioRxiv. 2021. doi: 10.1101/2021.08.30.458246
6 32. Stewart JA, Holland TC, Bhagwat AS. Human Herpes Simplex Virus-1 depletes
7 APOBEC3A from nuclei. Virology. 2019;537:104-9. doi: 10.1016/j.virol.2019.08.012.
8 33. Cheng AZ, Moraes SN, Attarian C, Yockteng-Melgar J, Jarvis MC, Biolatti M, Galitska
9 G, Dell'Oste V, Frappier L, Bierle CJ, Rice SA, Harris RS. A Conserved Mechanism of
10 APOBEC3 Relocalization by Herpesviral Ribonucleotide Reductase Large Subunits. Journal of
11 Virology. 2019;93(23). doi: 10.1128/jvi.01539-19.
12 34. Cheng AZ, Moraes SN, Shaban NM, Fanunza E, Bierle CJ, Southern PJ, Bresnahan WA,
13 Rice SA, Harris RS. APOBECs and Herpesviruses. Viruses. 2021;13(3):390. doi:
14 10.3390/v13030390.
15 35. Baek M, DiMaio F, Anishchenko I, Dauparas J, Ovchinnikov S, Lee GR, Wang J, Cong
16 Q, Kinch LN, Schaeffer RD, Millán C, Park H, Adams C, Glassman CR, DeGiovanni A, Pereira
17 JH, Rodrigues AV, Dijk AAv, Ebrecht AC, Opperman DJ, Sagmeister T, Buhlheller C, Pavkov-
18 Keller T, Rathinaswamy MK, Dalwadi U, Yip CK, Burke JE, Garcia KC, Grishin NV, Adams
19 PD, Read RJ, Baker D. Accurate prediction of protein structures and interactions using a three-
20 track neural network. Science. 2021;373(6557):871-6. doi: doi:10.1126/science.abj8754.
21 36. Münk C, Willemsen A, Bravo IG. An ancient history of gene duplications, fusions and
22 losses in the evolution of APOBEC3 mutators in mammals. BMC Evolutionary Biology.
23 2012;12(1):71. doi: 10.1186/1471-2148-12-71.

37. Larue RS, Jonsson SR, Silverstein KA, Lajoie M, Bertrand D, El-Mabrouk N, Hotzel I, Andresdottir V, Smith TP, Harris RS. The artiodactyl APOBEC3 innate immune repertoire shows evidence for a multi-functional domain organization that existed in the ancestor of placental mammals. BMC Molecular Biology. 2008;9(1):104. doi: 10.1186/1471-2199-9-104.

38. Ito J, Gifford RJ, Sato K. Retroviruses drive the rapid evolution of mammalianAPOBEC3genes. Proceedings of the National Academy of Sciences. 2020;117(1):610-8. doi: 10.1073/pnas.1914183116.

39. Conticello SG. The AID/APOBEC family of nucleic acid mutators. Genome Biology. 2008;9(6):229. doi: 10.1186/gb-2008-9-6-229.

40. Uriu K, Kosugi Y, Suzuki N, Ito J, Sato K. Elucidation of the Complicated Scenario of Primate APOBEC3 Gene Evolution. Journal of Virology. 2021;95(12):e00144-21.

41. McGeoch DJ, Cook S, Dolan A, Jamieson FE, Telford EA. Molecular phylogeny and evolutionary timescale for the family of mammalian herpesviruses. Journal of Molecular Biology. 1995;247(3):443-58. doi: 10.1006/jmbi.1995.0152.

42. Brito AF, Baele G, Nahata KD, Grubaugh ND, Pinney JW. Intrahost speciations and host switches played an important role in the evolution of herpesviruses. Virus Evolution. 2021;7(1):veab025.

43. Davison AJ. Evolution of the herpesviruses. Veterinary Microbiology. 2002;86(1-2):69-88. doi: 10.1016/s0378-1135(01)00492-8.

44. McGeoch DJ, Davison AJ. The molecular evolutionary history of the herpesviruses. Origin and Evolution of Viruses: Academic Press; 1999. p. 441-65.

45. Davison AJ. Comparative analysis of the genomes. Human herpesviruses: biology, therapy, and immunoprophylaxis: Cambridge University Press; 2007.

46. Shackelton LA, Holmes EC. The evolution of large DNA viruses: combining genomic information of viruses and their hosts. Trends in Microbiology. 2004;12(10):458-65. doi: 10.1016/j.tim.2004.08.005.

47. McGeoch DJ, Rixon FJ, Davison AJ. Topics in herpesvirus genomics and evolution. Virus Research. 2006;117(1):90-104. doi: 10.1016/j.virusres.2006.01.002.

48. Lembo D, Brune W. Tinkering with a viral ribonucleotide reductase. Trends in Biochemical Sciences. 2009;34(1):25-32. Epub 2008/11/05. doi: 10.1016/j.tibs.2008.09.008. PubMed PMID: 18990579.

49. Young LS, Rickinson AB. Epstein-Barr virus: 40 years on. Nature Reviews Cancer. 2004;4(10):757-68. doi: Epstein–Barr virus: 40 years on.

50. Koning FA, Newman ENC, Kim E-Y, Kunstman KJ, Wolinsky SM, Malim MH. Defining APOBEC3 Expression Patterns in Human Tissues and Hematopoietic Cell Subsets. Journal of Virology. 2009;83(18):9474-85. doi: doi:10.1128/JVI.01089-09.

51. Refsland EW, Stenglein MD, Shindo K, Albin JS, Brown WL, Harris RS. Quantitative profiling of the full APOBEC3 mRNA repertoire in lymphocytes and tissues: implications for HIV-1 restriction. Nucleic Acids Research. 2010;38(13):4274-84. doi: 10.1093/nar/gkq174.

52. Blasig C, Zietz C, Haar B, Neipel F, Esser S, Brockmeyer NH, Tschachler E, Colombini S, Ensoli B, Stürzl M. Monocytes in Kaposi's sarcoma lesions are productively infected by human herpesvirus 8. Journal of Virology. 1997;71(10):7963-8. doi: 10.1128/jvi.71.10.7963-7968.1997.

53. Caselli E, Galvan M, Cassai E, Caruso A, Sighinolfi L, Di Luca D. Human herpesvirus 8 enhances human immunodeficiency virus replication in acutely infected cells and induces

1 reactivation in latently infected cells. Blood. 2005;106(8):2790-7. doi: 10.1182/blood-2005-04-
2 1390.
3 54. Wu W, Vieira J, Fiore N, Banerjee P, Sieburg M, Rochford R, Harrington W, Feuer G.
4 KSHV/HHV-8 infection of human hematopoietic progenitor (CD34+) cells: persistence of
5 infection during hematopoiesis in vitro and in vivo. Blood. 2006;108(1):141-51. doi:
6 10.1182/blood-2005-04-1697.
7 55. Kim I-J, Flaño E, Woodland DL, Lund FE, Randall TD, Blackman MA. Maintenance of
8 long term γ-herpesvirus B cell latency is dependent on CD40-mediated development of memory
9 B cells. The Journal of Immunology. 2003;171(2):886-92. doi: 10.4049/jimmunol.171.2.886.
10 56. Chakraborty S, Valiya Veettil M, Chandran B. Kaposi's Sarcoma Associated Herpesvirus
11 Entry into Target Cells. Frontiers in Microbiology. 2012;3. doi: 10.3389/fmicb.2012.00006.
12 57. Salamango DJ, McCann JL, Demir Ö, Brown WL, Amaro RE, Harris RS. APOBEC3B
13 Nuclear Localization Requires Two Distinct N-Terminal Domain Surfaces. Journal of Molecular
14 Biology. 2018;430(17):2695-708. Epub 2018/05/19. doi: 10.1016/j.jmb.2018.04.044. PubMed
15 PMID: 29787764; PubMed Central PMCID: PMCPMC6456046.
16 58. Xiao X, Yang H, Arutiunian V, Fang Y, Besse G, Morimoto C, Zirkle B, Chen XS.
17 Structural determinants of APOBEC3B non-catalytic domain for molecular assembly and
18 catalytic regulation. Nucleic Acids Research. 2017;45(12):7494-506. doi: 10.1093/nar/gkx362.
19 PubMed PMID: 28575276; PubMed Central PMCID: PMCPMC5499559.
20 59. McCann JL, Cristini A, Law EK, Lee SY, Tellier M, Carpenter MA, Beghè C, Kim JJ,
21 Jarvis MC, Stefanovska B. R-loop homeostasis and cancer mutagenesis promoted by the DNA
22 cytosine deaminase APOBEC3B. bioRxiv2021.

60. Venkatesan S, Rosenthal R, Kanu N, McGranahan N, Bartek J, Quezada S, Hare J, Harris R, Swanton C. Perspective: APOBEC mutagenesis in drug resistance and immune escape in HIV and cancer evolution. Annals of Oncology. 2018;29(3):563-72.

61. Olson ME, Harris RS, Harki DA. APOBEC Enzymes as Targets for Virus and Cancer Therapy. Cell Chemical Biology. 2018;25(1):36-49. Epub 2017/11/16. doi: 10.1016/j.chembiol.2017.10.007. PubMed PMID: 29153851; PubMed Central PMCID: PMCPMC5775913.

62. Hayward JA, Tachedjian M, Cui J, Cheng AZ, Johnson A, Baker ML, Harris RS, Wang L-F, Tachedjian G. Differential evolution of antiretroviral restriction factors in pteropid bats as revealed by APOBEC3 gene complexity. Molecular Biology and Evolution. 2018;35(7):1626-37.

63. Jebb D, Huang Z, Pippel M, Hughes GM, Lavrichenko K, Devanna P, Winkler S, Jermiin LS, Skirmuntt EC, Katzourakis A. Six reference-quality genomes reveal evolution of bat adaptations. Nature. 2020;583(7817):578-84.

64. Wibbelt G, Kurth A, Yasmum N, Bannert M, Nagel S, Nitsche A, Ehlers B. Discovery of herpesviruses in bats. Journal of General Virology. 2007;88(10):2651-5.

65. Watanabe S, Maeda K, Suzuki K, Ueda N, Iha K, Taniguchi S, Shimoda H, Kato K, Yoshikawa Y, Morikawa S. Novel betaherpesvirus in bats. Emerging Infectious Diseases. 2010;16(6):986.

66. Wu Z, Ren X, Yang L, Hu Y, Yang J, He G, Zhang J, Dong J, Sun L, Du J. Virome analysis for identification of novel mammalian viruses in bat species from Chinese provinces. Journal of Virology. 2012;86(20):10999-1012.

67. Anthony SJ, Epstein JH, Murray KA, Navarrete-Macias I, Zambrana-Torrelio CM, Solovyov A, Ojeda-Flores R, Arrigo NC, Islam A, Ali Khan S. A strategy to estimate unknown viral diversity in mammals. MBio. 2013;4(5):e00598-13.

68. Sasaki M, Setiyono A, Handharyani E, Kobayashi S, Rahmadani I, Taha S, Adiani S, Subangkit M, Nakamura I, Sawa H. Isolation and characterization of a novel alphaherpesvirus in fruit bats. Journal of Virology. 2014;88(17):9819-29.

69. Sano K, Okazaki S, Taniguchi S, Masangkay JS, Puentespina R, Eres E, Cosico E, Quibod N, Kondo T, Shimoda H. Detection of a novel herpesvirus from bats in the Philippines. Virus Genes. 2015;51(1):136-9.

70. Zheng X-y, Qiu M, Chen S-w, Xiao J-p, Ma L-z, Liu S, Zhou J-h, Zhang Q-h, Li X, Chen Z. High prevalence and diversity of viruses of the subfamily Gammaherpesvirinae, family Herpesviridae, in fecal specimens from bats of different species in southern China. Archives of Virology. 2016;161(1):135-40.

71. Shabman RS, Shrivastava S, Tsibane T, Attie O, Jayaprakash A, Mire CE, Dilley KE, Puri V, Stockwell TB, Geisbert TW. Isolation and characterization of a novel gammaherpesvirus from a microbat cell line. Msphere. 2016;1(1):e00070-15.

72. Escalera-Zamudio M, Rojas-Anaya E, Kolokotronis S-O, Taboada B, Loza-Rubio E, Méndez-Ojeda ML, Arias CF, Osterrieder N, Greenwood AD. Bats, primates, and the evolutionary origins and diversification of mammalian gammaherpesviruses. MBio. 2016;7(6):e01425-16.

73. James S, Donato D, de Thoisy B, Lavergne A, Lacoste V. Novel herpesviruses in neotropical bats and their relationship with other members of the Herpesviridae family. Infection, Genetics and Evolution. 2020;84:104367.

74. Letko M, Seifert SN, Olival KJ, Plowright RK, Munster VJ. Bat-borne virus diversity, spillover and emergence. Nature Reviews Microbiology. 2020;18(8):461-71.

75. Lackey L, Law EK, Brown WL, Harris RS. Subcellular localization of the APOBEC3 proteins during mitosis and implications for genomic DNA deamination. Cell Cycle. 2013;12(5):762-72.

76. Schindelin J, Arganda-Carreras I, Frise E, Kaynig V, Longair M, Pietzsch T, Preibisch S, Rueden C, Saalfeld S, Schmid B, Tinevez JY, White DJ, Hartenstein V, Eliceiri K, Tomancak P, Cardona A. Fiji: an open-source platform for biological-image analysis. Nature Methods. 2012;9(7):676-82. Epub 2012/06/28. doi: 10.1038/nmeth.2019. PubMed PMID: 22743772; PubMed Central PMCID: PMCPMC3855844.

77. Stirling DR, Swain-Bowden MJ, Lucas AM, Carpenter AE, Cimini BA, Goodman A. CellProfiler 4: improvements in speed, utility and usability. BMC Bioinformatics. 2021;22(1):1-11.

78. Stirling DR, Carpenter AE, Cimini BA. CellProfiler Analyst 3.0: accessible data exploration and machine learning for image analysis. Bioinformatics. 2021;37(21):3992-4.

79. Edgar RC. MUSCLE: multiple sequence alignment with high accuracy and high throughput. Nucleic Acids Research. 2004;32(5):1792-7. doi: 10.1093/nar/gkh340.

80. Kumar S, Stecher G, Li M, Knyaz C, Tamura K. MEGA X: Molecular Evolutionary Genetics Analysis across Computing Platforms. Molecular Biology and Evolution. 2018;35(6):1547-9. doi: 10.1093/molbev/msy096.

81. Kumar S, Stecher G, Suleski M, Hedges SB. TimeTree: A Resource for Timelines, Timetrees, and Divergence Times. Molecular Biology and Evolution. 2017;34(7):1812-9. doi: 10.1093/molbev/msx116.

1

2 **Figure Legends**

3 **Fig. 1. Background on A3 counteraction by herpesvirus RNR subunits.**

4 (**A**) Schematic of EBV BORF2-mediated counteraction of A3B. BORF2 (red) directly binds A3B
5 (orange-green) and inhibits its ssDNA deaminase activity to protect viral genomes (blue) from
6 deamination during lytic replication. This interaction also results in relocalization of normally
7 nuclear A3B into cytoplasmic aggregates.

8 (**B**) Structure of A3A bound to ssDNA (pdb: 5SWW). L1, L3, and L7 regions are labelled and
9 colored in darker green. The aligned amino acid sequences of L1, L3, and L7 from A3A, A3Bctd,
10 and A3Gctd are shown on the right.

11 (**C**) Schematic of the human *A3* locus. These genes encode proteins with one or two zinc-
12 coordinating deaminase domains (Z domains), which belong to three classes based on sequence
13 similarity: Z1 (green), Z2 (orange), and Z3 (blue).

14 (**D**) Representative immunofluorescence microscopy images of HeLa T-REx cells transfected with
15 an empty vector control or the indicated FLAG-tagged RNR subunits (red) and incubated with
16 doxycycline to induce the expression of A3B-EGFP or A3A-EGFP (green). Cell nuclei are stained
17 using Hoechst 33342 (blue). Scale bars = 10 µm.

18

19 **Fig. 2. Involvement of the A3B and A3A loop 7 regions in binding to herpesvirus RNRs.**

20 (**A**) Co-immunoprecipitation of A3 L7 chimeras with EBV, KSHV, and HSV-1 RNR large
21 subunits. FLAG-tagged RNR subunits were co-expressed with the indicated A3-EGFP constructs
22 in 293T cells, affinity purified, and analyzed by immunoblotting to detect co-purifying A3
23 proteins.

(**B**) Representative immunofluorescence microscopy images of HeLa cells co-transfected with FLAG-tagged BORF2, ORF61, or ICP6 (red) and the indicated A3-EGFP constructs (green). Scale bars = 10 μm.

(**C**) Quantification of A3-EGFP relocalization in HeLa cells expressing the indicated herpesvirus RNR large subunits (n ≥ 100 cells per condition; mean ± SD for n = 3 independent experimental replicates).

Fig. 3. Role of A3B and A3A loop 3 in binding to herpesvirus RNRs.

(**A**) Co-immunoprecipitation of A3 L3 chimeras with EBV, KSHV, and HSV-1 RNR large subunits. FLAG-tagged RNR subunits were co-expressed with the indicated A3-EGFP constructs in 293T cells, affinity purified, and analyzed by immunoblotting to detect co-purifying A3 proteins.

(**B**) Representative immunofluorescence microscopy images of HeLa cells co-transfected with FLAG-tagged BORF2, ORF61, or ICP6 (red) and the indicated A3-EGFP constructs (green). Scale bars = 10 μm.

(**C**) Quantification of A3-EGFP relocalization in HeLa cells expressing the indicated herpesvirus RNR large subunits (n ≥ 100 cells per condition; mean ± SD for n = 3 independent experimental replicates).

Fig. 4. Role of A3B and A3A loop 1 in binding to herpesvirus RNRs.

(**A**) Co-immunoprecipitation of A3 L1 chimeras with EBV, KSHV, and HSV-1 RNR large subunits. FLAG-tagged RNR subunits were co-expressed with the indicated A3-EGFP constructs

in 293T cells, affinity purified, and analyzed by immunoblotting to detect co-purifying A3 proteins.

(**B**) Representative immunofluorescence microscopy images of HeLa cells co-transfected with FLAG-tagged BORF2, ORF61, or ICP6 (red) and the indicated A3-EGFP constructs (green). Scale bars = 10 μm.

(**C**) Quantification of A3-EGFP relocalization in HeLa cells expressing the indicated herpesvirus RNR large subunits (n ≥ 100 cells per condition; mean ± SD for n = 3 independent experimental replicates).

Fig. 5. EBV BORF2 interacts with A3Bctd loop 1 to inhibit DNA deaminase activity.

(**A**) Upper panels show DNA deaminase activity of extracts from HeLa T-REx cells transfected with the indicated FLAG-tagged RNR subunits and incubated with doxycycline to induce the expression of A3B-EGFP or A3A-EGFP. Lower panels show protein expression levels in the same extracts by immunoblotting.

(**B**) Top: Zoom-in of the BORF2-A3Bctd interface showing BORF2 Y481 (yellow) inserted between the L1 and α6 regions of A3Bctd (gray). Middle and bottom: predicted interfaces between ORF61 (pink)/ICP6 (blue) and A3Bctd (gray).

(**C**) Alternative view of the BORF2-A3Bctd interface highlighting BORF2 (yellow) interactions with A3Bctd L1 and L7 (gray).

(**D**) Upper panels show DNA deaminase activity of extracts from HeLa T-REx cells transfected the indicated FLAG-tagged BORF2 constructs and incubated with doxycycline to induce the expression of A3B-EGFP. Lower panels show protein expression levels in the same extracts by immunoblotting.

(**E**) Upper panels show DNA deaminase activity of extracts from HeLa cells co-transfected with FLAG-tagged EBV BORF2 and the indicated A3-EGFP constructs. Lower panels show protein expression levels in the same extracts by immunoblotting.

Fig. 6. Potential association between the genesis of *A3B* in primates and herpesvirus RNR evolution.

(**A**) Chronogram of primates depicting the generation of *A3B* in the common ancestor of hominoids and Old World monkeys. Primate groups shown in blue are composed of species that encode *A3B* and primates groups shown in red are composed of species that lack *A3B*. Primate phylogeny and divergence intervals were obtained from timetree.org [81]. Mya = million years ago.

(**B**) Top: Phylogram of human herpesviruses and indicated non-human primate herpesviruses based on RNR large subunit amino acid sequence. Shaded boxes indicate alpha-, beta-, and gamma-herpesvirus subfamilies. Genus classification is shown for gamma-herpesviruses. Gamma-herpesviruses that infect host species that encode *A3B* are shown in blue and those that infect host species that lack *A3B* are shown in red. Bottom: Host species infected by the indicated gamma-herpesviruses. Virus-host pairs are colored according to *A3B* status, as described above.

(**C**) Co-immunoprecipitation of human A3A and A3Bctd with the indicated RNR large subunits. FLAG-tagged RNR subunits were co-expressed with A3A-EGFP or A3Bctd-EGFP in 293T cells, affinity purified, and analyzed by immunoblotting to detect co-purifying A3 proteins. RNRs from viruses that infect host species that encode *A3B* are shown in blue and RNRs from viruses that infect host species that lack *A3B* are shown in red.

(**D**) Representative immunofluorescence microscopy images of HeLa T-REx cells transfected with the indicated FLAG-tagged RNR subunits (red) and incubated with doxycycline to induce the expression of human A3B-EGFP or A3A-EGFP (green). Scale bars = 10 μm.

(**E**) Upper panels show DNA deaminase activity of extracts from HeLa T-REx cells transfected with the indicated FLAG-tagged RNR subunits and incubated with doxycycline to induce the expression of A3B-EGFP or A3A-EGFP. Lower panels show protein expression levels in the same extracts by immunoblotting. RNRs from viruses that infect host species that encode *A3B* are shown in blue and RNRs from viruses that infect host species that lack *A3B* are shown in red.

A

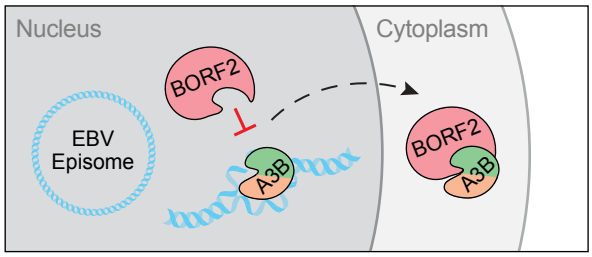

B

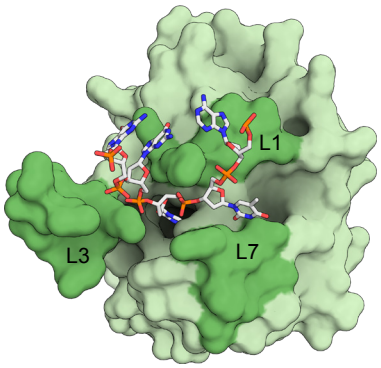

	L1
A3A -	G---IGRHK
A3Bctd -	DPLVLRRRQ
A3Gctd -	EPWVRGRHE

	L3
A3A -	KNLLCGFY
A3Bctd -	KNLLCGFY
A3Gctd -	PHKHGFLE

	L7
A3A -	YDPLYK
A3Bctd -	YDPLYK
A3Gctd -	DQGRCQ

C

Human *A3* locus

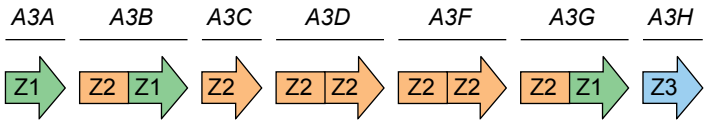

D

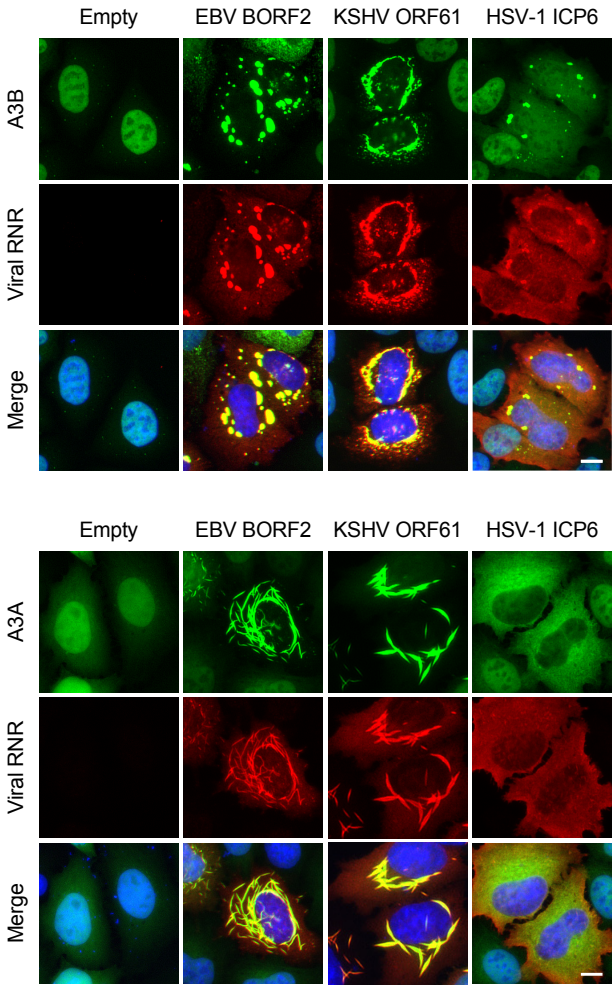

Moraes et al., Fig. 1

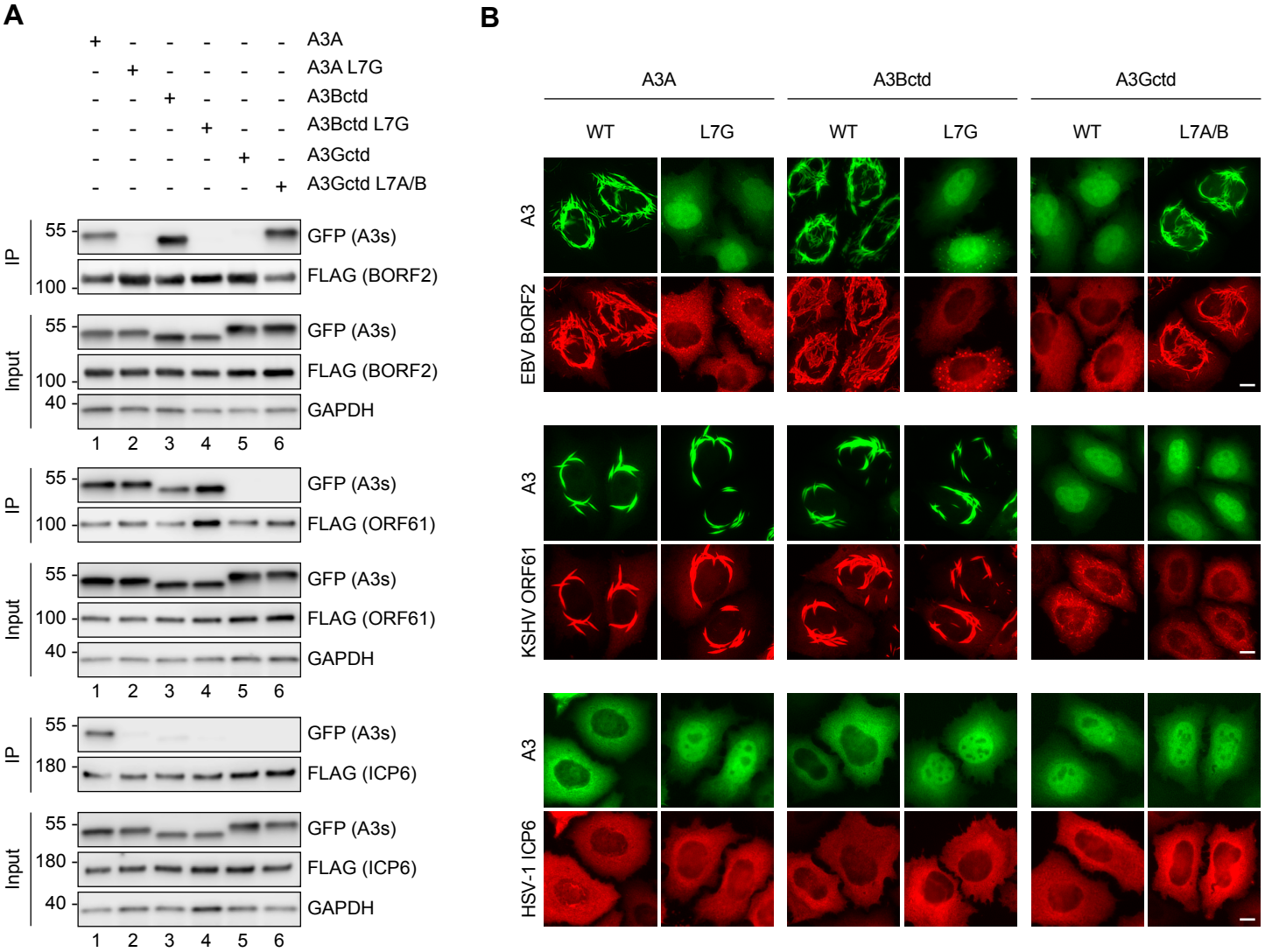

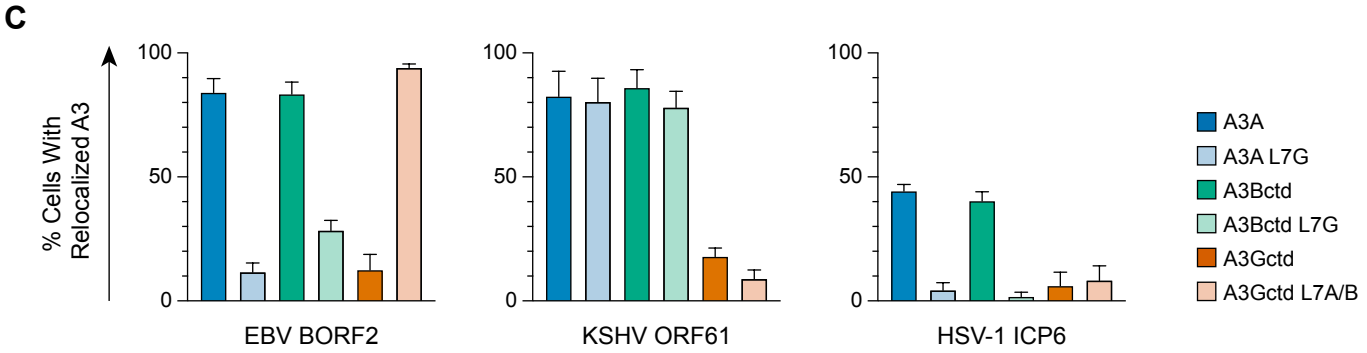

Moraes et al., Fig. 2

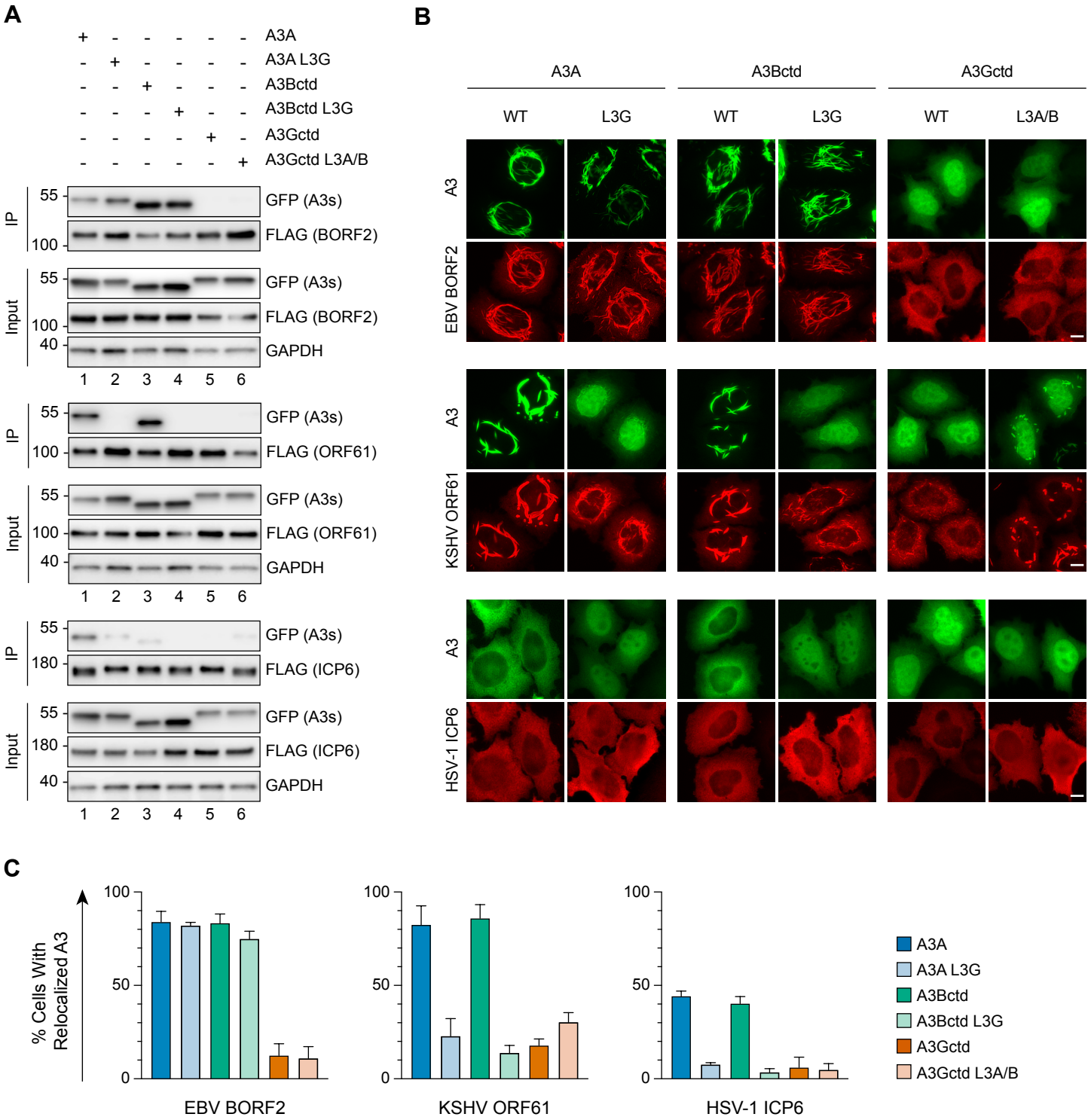

Moraes et al., Fig. 3

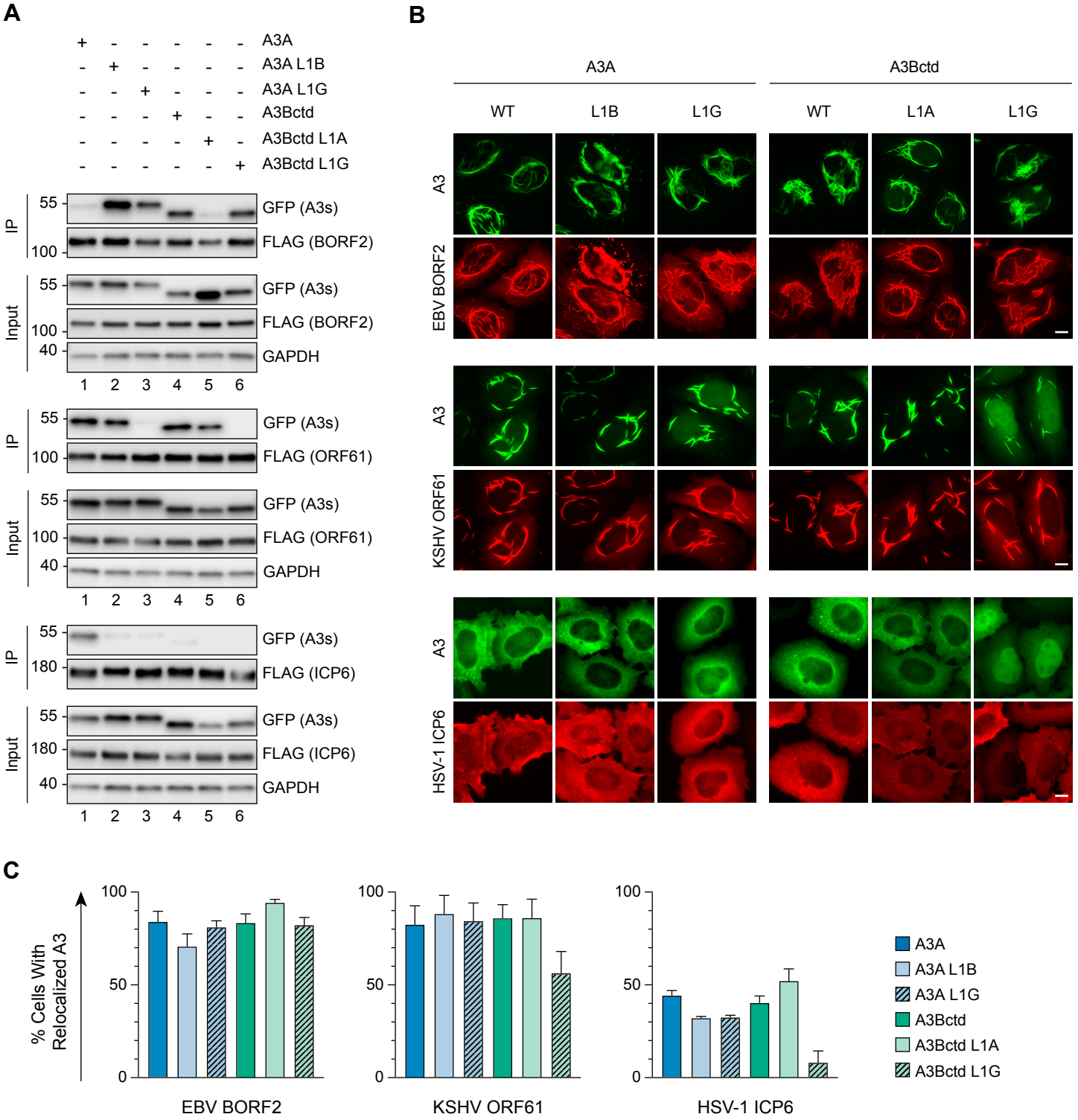

Moraes et al., Fig. 4

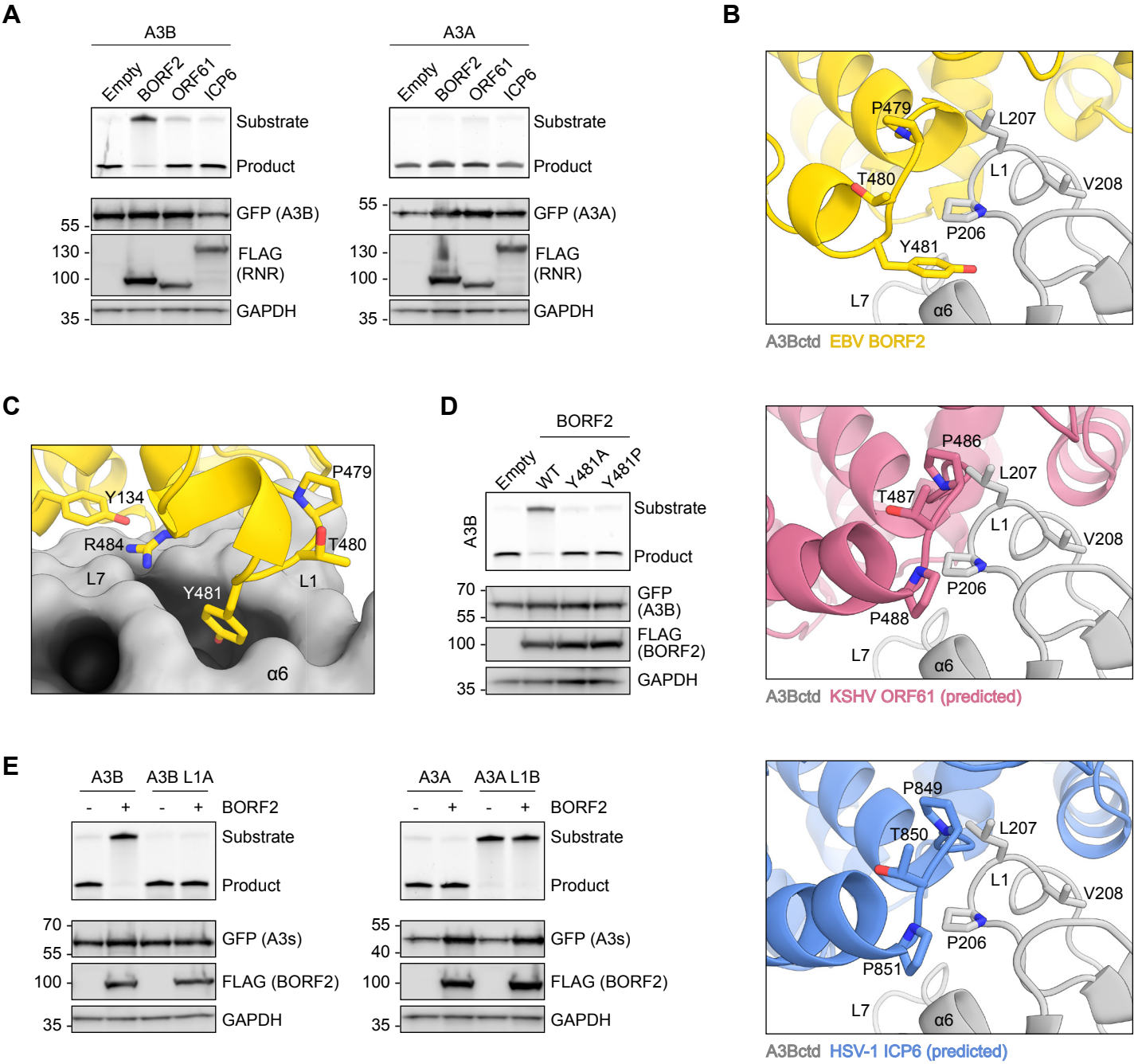

Moraes et al., Fig. 5

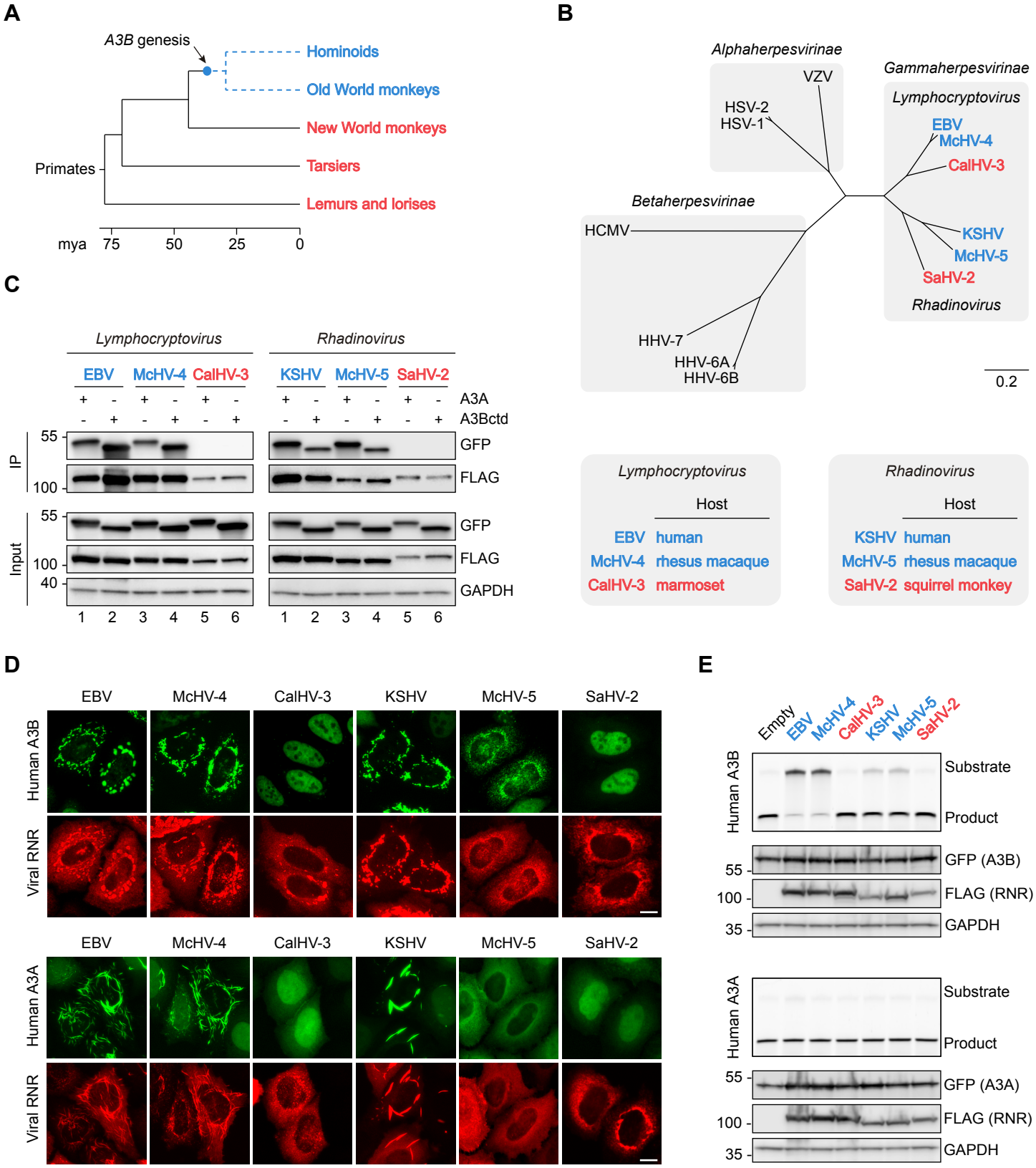

Moraes et al., Fig. 6